Numerical crisis found in the fixed step integration of a photoconductor model

Alicia Serfaty de Markus
Centro de Estudios Avanzados en Optica, Facultad de Ciencias, Universidad de los Andes, Mérida, Venezuela
(Received 21 January 1997)

A numerical examination is carried out on a theoretical model of irradiated intrinsic semiconductors. Depending on the integration artifact employed to solve the model, there are ''solutions'' that lead to a peculiar transient consisting of an intermittent chaotic dynamics that breaks down into a cascade of reverse period-doubling bifurcations. As such oscillatory instabilities are detrimental to photodetector performance, separation of the dynamics of the model from that of the numerics is crucial for the reliable design of these devices. This work characterizes these chaotic time series within the context of the potentially chaotic iterative structure that emerges from the discretization of the model. [S1063-651X(97)08806-5]

PACS number(s): 05.45.+b, 05.40.+j, 02.70.−c, 72.40.+w

INTRODUCTION

Illumination of a semiconductor with the proper wavelength unfolds a nonequilibrium complex kinetics that involves mainly the generation of electron-hole pairs by optical absorption, the annihilation of the pair through several recombination mechanisms, and the trapping of the carriers. Even in the purest samples, the contribution of the trapping level (or levels) in the recombination process is significant and decisive for examining the time-dependent behavior of charge carriers. In particular, chaotic oscillations in high-purity Ge, GaAs, and InSb have been detected under a wide variety of experimental conditions a number of years ago [1]. Yet there are aspects of the physical mechanism of these chaotic oscillations that are not well understood.

Here a realistic yet simplified mechanism is considered by neglecting the presence of deep centers and other types of defects states. In the present model we have assumed only one type of shallow trap, which strongly dominates the recombination process. This situation is very common and is reflected in samples where the photoluminescense peak is located on the low-energy side of the band edge and is very intense compared to the peak corresponding to the band-gap transition. The rate equations for the electron transitions of the photoconducting process outlined above are given by

$$\frac{dn}{dt} = G - n\alpha_1(N_t - m) + \gamma_1 m - c_1 n,$$

$$\frac{dm}{dt} = n\alpha_1(N_t - m) - \delta_0 mp - \gamma_1 m, \qquad (1)$$

$$\frac{dp}{dt} = G - \delta_0 mp - c_2 p,$$

where n and p are the free electron and hole densities and m is the trapped electron density at the trap at time t. A more detailed description of the physical meaning of the seven parameters present in Eq. (1) is given in Ref. [2].

The essential physical process of photoconduction in intrinsic semiconductors is based on the interplay between the generation and recombination or trapping of charge carriers; so it could be realized that the dynamics of the system may become complicated, in particular for high intensity of radiation, and the possibility of chaotic oscillations is present. Moreover, for the nonlinear photoconductor equations (1) there is no analytical solution and then numerical integration techniques have to be employed, such as the single-step Runge-Kutta (RK) method or the multistep Gear method. Further, in the event that the present system (1) becomes stiff, the numerical integration is not a straightforward task, as the numerical outcome depends strongly on the type of scheme employed; see Ref. [3].

Figure 1(a) shows the time series for the free-electron population (here the lines joining the successive data points were omitted). This result was obtained with a fourth-order RK integration of system (1) and typically consists of a transient with an intermittent chaotic stage followed by a cascade

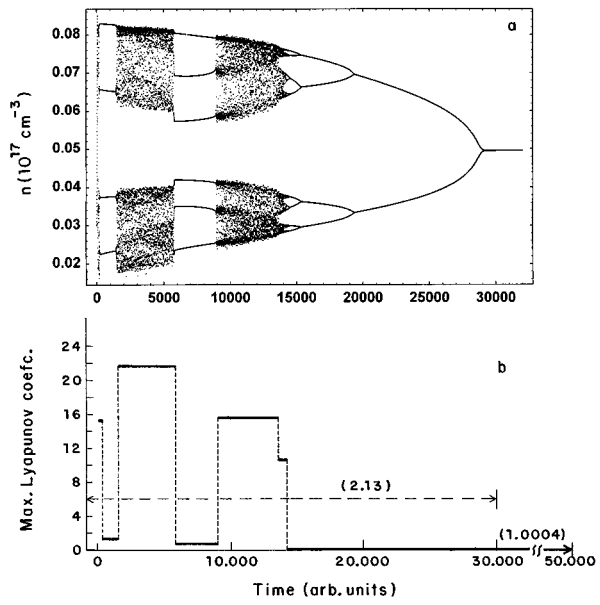

FIG. 1. (a) Complete transient of the free electrons obtained with the RK algorithm for $\alpha_1 = 4.1 \times 10^{-14}\ \mathrm{cm}^{-3}\,\mathrm{s}^{-1}$ and $h = 0.01$. (b) Maximum Lyapunov coefficient for the indicated regions in the transient. In parentheses is the Lyapunov dimension for the whole transient and after it has ceased.

of reversal bifurcations that converges into the system fixed points. The convergence of this reverse process actually corresponds to a reverse period-doubling or period-halving bifurcation. By inspection of Fig. 1(a), as the time progresses, the ratio of the successive onset values (except the last one) follows closely the Feigenbaum number. In the same way, the ratio of the successive (reverse) branch splitting follows the corresponding scaling number [4]. This peculiar behavior disappears completely when integrating Eq. (1) with an adaptive algorithm such as the Gear or the Adam-Moulton scheme, which constitutes direct evidence that the observed chaotic transient of Fig. 1(a) has been numerically induced [3].

The technological importance of photoconductivity, particularly its applications in high-speed and far-infrared photodetectors and similar devices, leads to the need for a careful investigation of the charge-carrier dynamics. More specifically, in order to accomplish a *reliable* design on real devices based on model (1) or similar models (if extended to include, for instance, more trapping levels and recombination centers), it becomes critical to recognize whether the observed irregular transient is due to the nonlinear nature of the rate equations (1) or it has a purely numerical origin.

Now, despite the fact that there has been an increasing amount of work devoted to the study of numerically induced chaos [5,6], those studies have focused mainly on the conventional asymptotic chaos. This work examines the photoconductor transient response, and with the help of techniques usually employed in the study of asymptotic chaos, a portrayal of the chaotic transient is constructed, pointing out some possible causes of this amazing behavior.

EXPERIMENTAL PROCEDURE

The photoconductor equations (1) were evaluated by setting the parameters values as $G=10^{16}$ electron-hole pairs per $\mathrm{cm}^2\,\mathrm{s}$, $N_t=10^{14}\ \mathrm{cm}^{-3}$, $c_1=1.5\times10^{-3}\ \mathrm{s}^{-1}$, $c_2=1.5\times10^{-5}\ \mathrm{s}^{-1}$, $\delta_0=10^{-15}\ \mathrm{cm}^{-3}\,\mathrm{s}^{-1}$, and $\gamma_1=0.83\ \mathrm{s}^{-1}$. The ''parameter of control'' in this study will be the probability of capture to the traps α_1. The parameter α_1 is physically significant as it is sensitive to the temperature and homogeneity of the sample. Therefore, the variation in it should be examined. The initial conditions for conduction electrons, trapped electrons, and holes are, respectively, $n_0=3\times10^{15}\ \mathrm{cm}^{-3}$, $m_0=10^{10}\ \mathrm{cm}^{-3}$, and $p_0=5\times10^{13}\ \mathrm{cm}^{-3}$. The numerical integration of system (1) was carried out by means of the classical fourth-order Runge-Kutta method.

Basically, the RK technique is constructed with a truncated Taylor series where the evaluation of the higher-order derivatives are replaced by a set of formulas based on the more fundamental explicit Euler algorithm [7]. Here intermediate points are used to calculate the state at time t_{k+1}. This idea is easily observable for the second-order RK recursion formula

$$x_{k+1}=x_k+hf\left(t_k+\tfrac{1}{2}h,x_k+\tfrac{1}{2}hf(x_k,t_k)\right), \tag{2}$$

where $h>0$ is the step size and $f(x_k,t_k)$ is the vector field value.

It can be shown [8] that expression (2) reproduces a Taylor series up to the second-order term. Similarly, the fourth-order RK reproduces a Taylor series up to the fourth term. Here, for simplicity, the second-order RK recursion formula (2) is applied to system (1), leading to the expressions

$$\begin{aligned} n_{k+1}&=n_k+hf_1(t_k+\tfrac{1}{2}h,n_k+\tfrac{1}{2}k_1,m_k+\tfrac{1}{2}l_1,p_k+\tfrac{1}{2}r_1),\\ m_{k+1}&=m_k+hf_2(t_k+\tfrac{1}{2}h,n_k+\tfrac{1}{2}k_1,m_k+\tfrac{1}{2}l_1,p_k+\tfrac{1}{2}r_1),\\ p_{k+1}&=p_k+hf_3(t_k+\tfrac{1}{2}h,n_k+\tfrac{1}{2}k_1,m_k+\tfrac{1}{2}l_1,p_k+\tfrac{1}{2}r_1), \end{aligned} \tag{3}$$

where, according to the photoconductor rate equations (1), k_1, l_1, and r_1 are defined, respectively, as

$$\begin{aligned} k_1&=hf_1(t_k,n_k,m_k,p_k)\\ &=h[G-n_k\alpha_1(N_t-m_k)+\gamma_1 m_k-c_1n_k],\\ l_1&=hf_2(t_k,n_k,m_k,p_k)\\ &=h[n_k\alpha_1(N_t-m_k)-\delta_0m_kp_k-\gamma_1m_k],\\ r_1&=hf_3(t_k,n_k,m_k,p_k)=h(G-\delta_0m_kp_k-c_2p_k). \end{aligned} \tag{4}$$

In particular, for the electron population, the corresponding vector field f_1 is given as

$$\begin{aligned} f_1(t_k+\tfrac{1}{2}h,n_k+\tfrac{1}{2}k_1,m_k+\tfrac{1}{2}l_1,p_k+\tfrac{1}{2}r_1)&\\ =G-(n_k+\tfrac{1}{2}k_1)\alpha_1[N_t-(m_k+\tfrac{1}{2}l_1)]&\\ +\gamma_1(m_k+\tfrac{1}{2}l_1)-c_1(n_k+\tfrac{1}{2}k_1),& \end{aligned} \tag{5}$$

replacing the values of k_1 and l_1 given in Eq. (4) into Eq. (5) for f_1,

$$\begin{aligned} f_1=G&-\{n_k+\tfrac{1}{2}h[G-n_k\alpha_1(N_t-m_k)+\gamma_1m_k-c_1n_k]\}\alpha_1\\ &\times(N_t-\{m_k+\tfrac{1}{2}h[n_k\alpha_1(N_t-m_k)-\delta_0m_kp_k-\gamma_1m_k]\})\\ &+\gamma_1\{m_k+\tfrac{1}{2}h[n_k\alpha_1(N_t-m_k)-\delta_0m_kp_k-\gamma_1m_k]\}\\ &-c_1\{n_k+\tfrac{1}{2}h[G-n_k\alpha_1(N_t-m_k)+\gamma_1m_k-c_1n_k]\}. \end{aligned} \tag{6}$$

Solving the innermost products appearing in Eq. (6) gives

$$\begin{aligned} f_1=G&-(n_k+\tfrac{1}{2}hG-\tfrac{1}{2}hn_k\alpha_1N_t+\tfrac{1}{2}hn_k\alpha_1m_k+\tfrac{1}{2}h\gamma_1m_k\\ &-\tfrac{1}{2}hc_1n_k)(\alpha_1N_t-\alpha_1m_k-\tfrac{1}{2}h\alpha_1^2n_kN_t+\tfrac{1}{2}h\alpha_1^2n_km_k\\ &+\tfrac{1}{2}h\alpha_1\delta_0m_kp_k+\tfrac{1}{2}h\alpha_1\gamma_1m_k)+\gamma_1m_k+\tfrac{1}{2}h\alpha_1n_kN_t\gamma_1\\ &-\tfrac{1}{2}h\alpha_1n_km_k\gamma_1-\tfrac{1}{2}h\delta_0m_kp_k\gamma_1-\tfrac{1}{2}hm_k\gamma_1^2-c_1n_k\\ &-\tfrac{1}{2}hc_1G+\tfrac{1}{2}hc_1n_k\alpha_1N_t-\tfrac{1}{2}hc_1n_k\alpha_1m_k\\ &-\tfrac{1}{2}hc_1\gamma_1m_k+\tfrac{1}{2}hc_1^2n_k. \end{aligned} \tag{7}$$

Now, when solving the cross products from Eq. (7), second-order terms for n_k will appear. The vector field value f_1 of Eq. (7) can be expressed briefly as

$$f_1=f_1'(n_k,m_k)+g_1(m_k)+C_1, \tag{8}$$

where f_1' contains all terms involving the factor n_k, g_1 contains the terms involving only the factor m_k, and all remnant terms not involving the charge carrier variables are grouped as a ''constant'' term C_1. Substituting Eq. (8) in Eq. (3), the expression for the $k+1$ iterate of the discretized electron population is given as

$$n_{k+1}=n_k+hf_1=n_k+h[n_kF_1(n_k,m_k)+g_1(m_k)+C_1], \tag{9}$$

where the function F_1 results after taking n_k as a common factor in f_1', i.e., $f_1'=n_kF_1(n_k,m_k)$. Rewriting Eq. (9) and extending for all charge carriers,

$$\begin{aligned} n_{k+1}&=n_k[1+hF_1(n_k,m_k)]+hg_1(m_k)+hC_1,\\ m_{k+1}&=m_k[1+hF_2(n_k,m_k,p_k)]+hg_2(p_k,n_k)+hC_2, \\ p_{k+1}&=p_k[1+hF_3(m_k,p_k)]+hg_3(m_k)+hC_3, \end{aligned} \tag{10}$$

where F_i contains the respective first-order terms for the discretized variable. As in F_1, the variables in F_2 and F_3 depend on those present in f_2 and f_3, respectively; see Eq. (4). The second term of Eq. (10) represents coupling expressions g_i and the constant terms C_i may play a role in the bifurcation reversals, to be discussed later.

After some simple transformations, it is possible to see that the first terms of the recursive formulas (10) are structurally similar to the recursive formula of the well-known logistic map $x_{k+1}=\mu x_k(1-x_k)$ [9], with μ as a parameter. This similitude should account for the intermittent chaotic behavior observed in the time series of Eq. (1) for certain parameters values, analogous to the logistic map displaying chaos through period-doubling bifurcations in the μ vs x_k plot for certain values of the μ parameter. As discussed in Ref. [3] for a simple nonlinear equation, the emergence of factors of the form nh in the recursion formulas such as Eq. (10) will play the same ''parameter'' role in the time domain as μ in the parameter domain.

RESULTS AND DISCUSSION

For variations of the parameter of control α_1, it was observed that the photoconductor equations (1) becomes stiff since increasing the capture probability amplifies not only the separation of time scales for the charge carriers, but also the slower and faster components of each variable. For a stiff system the stability of system (1) and thus of the RK algorithm will be greatly affected depending on the size of the step chosen [7]. With a fixed step of $h=0.01$ for the RK integrator and increasing the capture probability, the changes observed in the transient response for electrons follow from monotonic (i.e., exponential type, $\alpha_1=5\times10^{-16}\ \mathrm{cm^{-3}\,s^{-1}}$) to (quasi)periodic ($\alpha_1=6\times10^{-15}\ \mathrm{cm^{-3}\,s^{-1}}$) to irregular chaotic oscillations ($\alpha_1=4\times10^{-14}\ \mathrm{cm^{-3}\,s^{-1}}$) and finally to numerical overflow ($\alpha_1>4.65\times10^{-14}\ \mathrm{cm^{-3}\,s^{-1}}$). Physically, as α_1 grows, there is an enhancement of the trapping action, which competes significantly with the generation and recombination of charge carriers. Thus these simultaneous competitive processes affect the separation of time scales during the time evolution for each variable and between the variables, producing a strong stiffness over the system. In this situation, the algorithm becomes unstable, affecting mainly the transient response for the charge carriers, as shown in Fig. 1(a). The collective behavior for the n, m, and p populations is better visualized in the phase plot shown in Fig. 2 for $\alpha_1=4.1\times10^{-14}\ \mathrm{cm^{-3}\,s^{-1}}$ and $h=0.01$. This process of the photoconductor becoming stiff with the α_1 parameter is consistent with some of the eigenvalues growing towards positive values, as reported in Ref. [10]. It is worth mentioning that in this study, besides the capture probability, similar chaotic response has been observed with variations of the radiation intensity G, the probability of ejection from the traps γ_1, and the density of traps N_t.

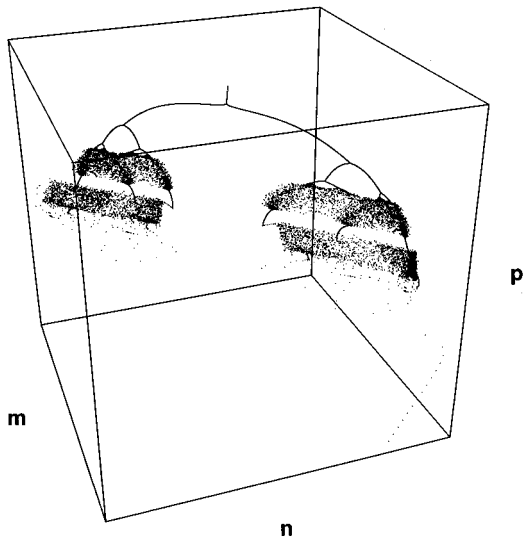

FIG. 2. Repeller found in phase space for $\alpha_1=4.1\times10^{-14}\ \mathrm{cm^{-3}\,s^{-1}}$ for the RK algorithm with $h=0.01$.

Evidence that the irregular transients, such as those shown in Figs. 1(a) and 2, are indeed chaotic can be found in several ways: first, by means of the return map for any of the variables n, m, or p of system (1); second, by the corresponding power spectrum density; third, by the sensitivity to initial conditions for a chaotic system; and finally, by the detection of positive Lyapunov exponents.

Figure 3 shows the first-return map for the density of trapped electrons for $\alpha_1=4.1\times10^{-14}\ \mathrm{cm^{-3}\,s^{-1}}$ and $h=0.01$. Here it is possible to appreciate that the irregular oscillations of the transient are not random but chaotic, as all the orbits are (partially) attracted to the nonperiodic object showed in Fig. 3 (repeller) in the same manner as to the three-dimensional object of Fig. 2.

The frequency analysis of the time series was carried out

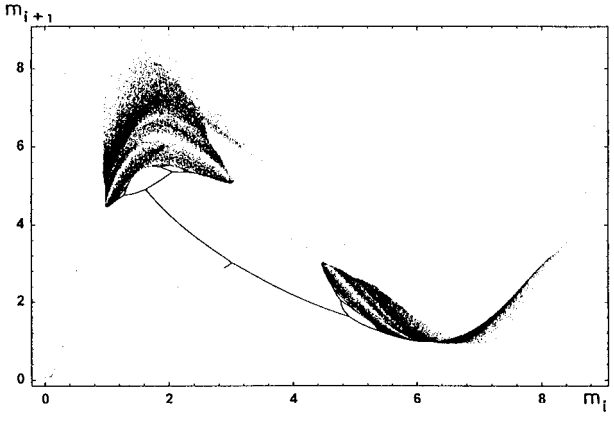

FIG. 3. First-return map of the trapped electrons for $\alpha_1=4.64\times10^{-14}\ \mathrm{cm^{-3}\,s^{-1}}$ and $h=0.01$, showing a chaotic repeller for the trapped charge carrier.

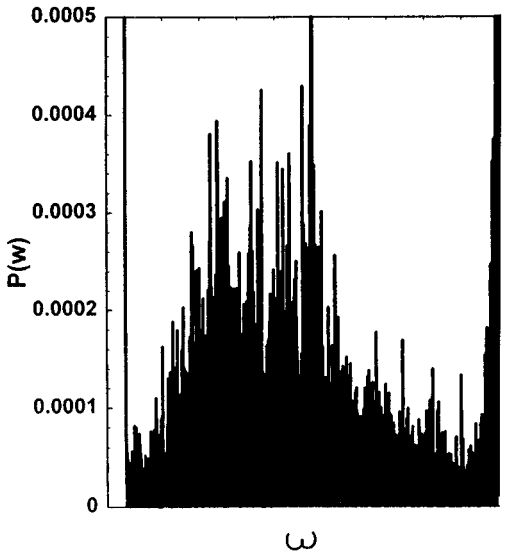

FIG. 4. Power spectrum density of the free electrons for $\alpha_1 = 4.64\times10^{-14}\ \mathrm{cm^{-3}\,s^{-1}}$ and $h=0.01$, showing a background of the continuous spectrum.

for increasing values of the capture probability. A widening of the power spectrum was observed characterized by an increasing broadband noise as the transient becomes chaotic. Figure 4 shows the power spectrum density for the density of electrons for $\alpha_1 = 4.64\times10^{-14}\ \mathrm{cm^{-3}\,s^{-1}}$ and $h=0.01$, where there are some wide peaks on a background of continuous spectrum, indicating the presence of a strange attractor (i.e., strange repulser in this case).

The characteristic sensitivity to initial conditions expected in chaotic regimes was observed in the photoconductor system (1). Figure 5 shows a distinctive change in the response for the density of electrons to slight changes on the initial conditions, such as $n_0 = 9.530\,51\times10^{14}$ and $9.530\,510\,08\times10^{14}\ \mathrm{cm^{-3}}$ for $h=0.05$. This last aspect was particularly enhanced for the larger step sizes, as expected consistently with the numerical origin of this chaotic dynamics.

Lyapunov characteristic exponents are quantities used to quantify the erratic or chaotic behavior of a system's dynamics. They play a crucial role in the description of the behavior of a dynamical system, as they are used to measure divergence or convergence from a nearby initial point, that is, to check the sensitive dependence on initial conditions in order to detect the presence of chaotic attractors. If we consider a small hypersphere of initial conditions in the phase space, for sufficiently short time scales, the effect of the dynamics will be to distort this set into a hyperellipsoid, stretched along some directions and contracted along others. Each Lyapunov coefficient quantifies the average exponential rate of expansion or contraction for a given direction (axis). Thus, if there is at least one positive Lyapunov coefficient, it represents a measure of how chaotically the system behaves. The rate of expansion of the largest axis, corresponding to the most unstable direction of the flow, is measured by the largest Lyapunov coefficient.

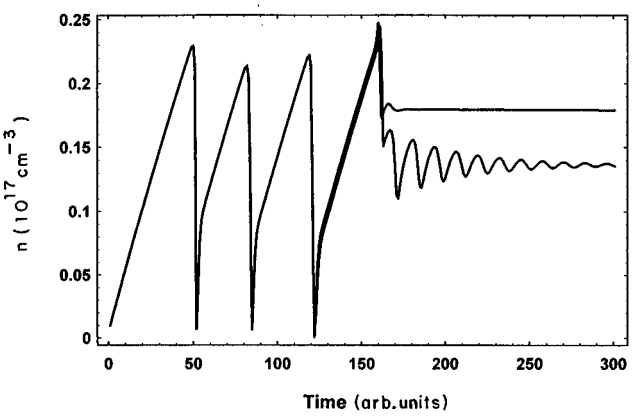

FIG. 5. Sensitivity to the initial conditions of the free electrons for the larger step sizes for $\alpha_1 = 2.5\times10^{-15}\ \mathrm{cm^{-3}\,s^{-1}}$ and $h=0.05$. The upper curve is for $n_0 = 9.530\,51\times10^{14}\ \mathrm{cm^{-3}}$ and the lower for $n_0 = 9.530\,510\,08\times10^{14}\ \mathrm{cm^{-3}}$.

However, Lyapunov exponents are an *asymptotic* measure of such behavior. Nevertheless, in this study an attempt was made to measure the whole Lyapunov spectrum for defined regions of the transient, as indicated in Fig. 1(b), as well as the Lyapunov dimension. Such an attempt was carried out by taking advantage of the improved algorithm of Bennetin, Galgani, and Strelcyn [11] for the evaluation of the Lyapunov spectrum and care was taken that enough data points were taken from the time series as to ensure convergence of the Lyapunov exponents. This procedure was possible as this algorithm permits one to take arbitrarily short time intervals and repeat the integration orthonormalization [11] procedure the necessary number of times to cover the region to be studied. The resulting spectrum was composed of three coefficients, as expected for the system of equations (1). Results are shown in Fig. 1(b) for the maximum Lyapunov exponent, which turn out to be positive within the chaotic regions, in agreement with the chaotic dynamics, and practically zero inside the periodic windows and the bifurcation region of Fig. 1(a). The second and third Lyapunov exponents were always negative and nonvanishing, as expected for trajectories with fixed point attractors [12], as in the present case.

The ''dimension'' of a system being observed corresponds to the number of independent quantities needed to specify the state of the system at any given instant. Thus the observed dimension of an attractor is the number of independent quantities needed to specify a point on the attractor. In a chaotic attractor this dimension is directly related to the number of non-negative characteristic Lyapunov exponents; according to the relation [11]

$$D_L = j - \left(\sum_{i=1}^{j} \lambda_i\right) \Big/ \lambda_{j+1}, \tag{11}$$

where the Lyapunov coefficients λ_i are ordered as $\lambda_1 \geqslant \cdots \geqslant \lambda_n$ and j is the largest integer such that $\lambda_1 + \cdots + \lambda_j > 0$.

The Lyapunov dimension D_L, which is related to the fractal dimension of the attractor (repeller in this case), was found to be 2.13 for the whole transient up to period one. This dimension gives a lower bound for the number of independent variables of the system; thus the value obtained in this study between 2 and 3 is in complete agreement with the three-dimensional photoconductor model. This dimension is

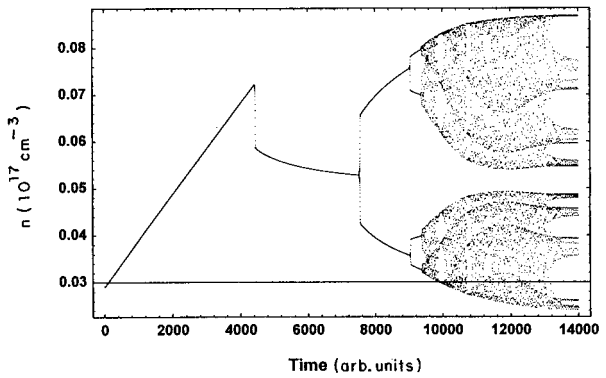

FIG. 6. First 14 000 points of the time series for $\alpha_1 = 4 \times 10^{-12}$ cm^{-3} s^{-1} and $h = 0.0001$, showing that chaotic oscillations begin as a bifurcation process according to an antimonotonic process.

somewhat higher than the previously calculated dimension for the very similar Lorenz model [9], with a Lyapunov dimension of 2.07 [13], a result to be expected since only two of the three Lorenz equations are nonlinear. For the periodic regions of Fig. 1(a) a Lyapunov dimension very close to one was obtained; see Fig. 1(b).

As pointed out in Ref. [3], discretization through a RK routine of the photoconductor equations (1) may lead to a numerical induced chaos related to the homoclinical structure associated with the system. Such situation have been precisely studied in certain models [5,6]. However, it is far from obvious why in the photoconductor case the chaotic behavior is confined to a transient form, reversing to a stable asymptotic state by period-doubling bifurcations. Nevertheless, such reverse period-doubling processes are not uncommon.

Evidence for systems that suppress chaos through reverse bifurcations are found in many cases. This reversals have been discussed before by Stone [14], proposing that this remarkable situation is found for a certain class of functions. This phenomenon is to be expected much more frequently in higher-order systems. In general, in a reverse bifurcation process the transition from chaos to order is presumably due to some structural (small) perturbation, which is incorporated as a term added to the original function [14]. The family of functions with an added perturbation displays initially a bifurcation structure. Next a critical stage is reached, where an infinite number of fixed points emerge and the population dynamics becomes chaotic; then an ordered sequence of periodic windows is entered until finally all chaos is removed through reversals to reach a period one for the steady state (as in Figs. 1 and 2). This description fits the observed behavior displayed in Figs. 1 and 6 for the first 14 000 points of the time series for $\alpha_1 = 4 \times 10^{-12}$ cm^{-3} s^{-1} and $h = 0.0001$. For the photoconductor case, it is possible to speculate that the origin of the perturbation in the photoconductor could be traced to the remnant constant terms appearing in the discretized equation (10). These remaining terms build up in each successive iteration of the explicit RK algorithm. On the other hand, none of these effects are to be expected for the multistep–variable-step implicit Gear algorithm because error is much better controlled [7].

The reversal breakdown of chaos through period halving may cause the bifurcation diagram to ''bubble,'' that is, the appearance of certain structures formed by the process of bifurcation and reversals. Mathematically speaking, this kind of behavior is known as antimonotonicity [15]. As for Fig. 6, it is possible to appreciate that the chaotic oscillations actually begin as a bifurcation process. Considering that the photoconductor transient ends as a cascade of reversals [see Fig. 1(a)], the whole transient may be regarded structurally as a bubble. That is, the transient evolves according to an antimonotonic process. This is in agreement with models in two or higher dimensions that show suppression of chaos through a reverse bifurcation by antimonotonic behavior [14–16].

Another approach to explain the suppression of chaos comes directly from the very concept of chaotic transient, extensively studied by Grebogi and OH [17] and Tel [18]. In the context of the trajectories followed by system (1) in phase space (see Fig. 2), as it evolves with time, the term chaotic transient refers to the fact than an orbit can spend a long time in the neighborhood of a nonattracting chaotic set before it leaves, possibly moving off to some nonchaotic attractor that governs its motion thereafter. In the photoconductor, the nonattracting chaotic set corresponds to the repeller (the intermittent region) and the nonchaotic attractor corresponds to the fixed point attractors (period-one attractors), reached after the stage of inverse period-doubling bifurcations. This rather sudden change from chaotic to nonchaotic attractor is most probably due to a ''crisis''; see Ref. [17] for a detailed description. Moreover, the time the orbit spends on the chaotic transient depends sensitively on its initial conditions [18]. Thus it is expected for a chaotic transient that the duration of the transient (escape time) has a characteristic average lifetime that follows a power law with a parameter [17,19]. In fact, such a dependence was observed in the present study. However, in Ref. [20] it was found that when varying two independent parameters of the photoconductor model (1), the corresponding escape time followed a power-law dependence with each parameter, but with exactly the *same* critical exponent; this parallelism is considered thus as further evidence of the numerical source underlying the chaotic transients. Thus, in the context of suppression of chaos through a crisis according to Ref. [17], the breakdown of the numerically induced photoconductor chaotic transients could be related to the controversial idea of a ''numerical crisis.''

CONCLUSION

The dynamics of a photoconductor model constructed with a set of nonlinear coupled ordinary differential equations has been examined. It was found that in the event that the system of equations becomes stiff, numerical integration with fixed step schemes produces a complex transient consisting of an intermittent regime followed by a cascade of period-doubling reverse bifurcations. It was concluded that the observed dynamics was indeed chaotic as it conforms to the characteristic features expected in a chaotic regime. Such behavior is undesirable for the performance of photoconductor devices and may restrict the range of material parameters for which chaotic oscillations can be expected. Instead, it was shown that application of a RK scheme over the photo-

conductor model leads to a nonlinear iterative structure, that may become responsible for the chaotic behavior observed. This opens the possibility of a homoclinic structure associated with the photoconductor equations, which may belong to a certain family of functions that suppress chaos with bifurcations reversals through an antimonotonic numerical crisis. Therefore, it is critical to evaluate as well the numerical impact over a theoretical model applied in the development of a given device.

ACKNOWLEDGMENT

This work was supported by the Consejo de Desarrollo Cientifico de la Universidad de Los Andes under Project No. C-621-93A.

[1] E. Schöll, Phys. Rev. B **34**, 1395 (1986).
[2] A. Serfaty and N. V. Joshi, Phys. Rev. B **47**, 3983 (1993).
[3] A. Serfaty de Markus, J. Comput. Phys. **132**, 409 (1997).
[4] M. Feigenbaum, Los Alamos Sci. **1**, 4 (1980).
[5] M. J. Ablowitz and B. M. Herbst, SIAM (Soc. Ind. Appl. Math.) J. Appl. Math. **50**, 339 (1990).
[6] P. K. Yee, P. K. Sweby, and D. F. Griffiths, J. Comput. Phys. **97**, 249 (1991).
[7] T. S. Parker and L. O. Chua, in *Practical Numerical Algorithms for Chaotic Systems* (Springer-Verlag, New York, 1989).
[8] F. Scheid, *Numerical Methods* (McGraw-Hill, New York, 1991).
[9] E. Ott, *Chaos in Dynamical Systems* (Cambridge University Press, Cambridge, 1993).
[10] A. Serfaty de Markus and N. V. Joshi, Chaos Solitons Fractals **7**, 1095 (1996).
[11] G. Bennetin, A. Galgani, and J. M. Strelcyn, Meccanica **15**, 21 (1980); M. Sandri, Math. J. **6**, 78 (1996).
[12] H. Haken, Phys. Lett. **94A**, 71 (1983).
[13] A. Wolf, J. Swift, H. Swinney, and J. Vastano, Physica D **16**, 285 (1985).
[14] L. Stone, Nature (London) **365**, 617 (1993).
[15] I. Kan and J. A. York, Bull. Am. Math. Soc. **23**, 469 (1990).
[16] S. P. Dawson, C. Grebogi, J. A. Yorke, I. Kan, and H. Kocak, Phys. Lett. A **162**, 249 (1992).
[17] C. Grebogi and E. Ott, Physica D **7**, 181 (1983).
[18] T. Tèl, in *Transient Chaos, Directions in Chaos*, edited by Hao Bai-Lin (World Scientific, Singapore, 1990), Vol. 3, pp. 149–211.
[19] S. P. Dawson and C. Grebogi, Chaos Solitons Fractals **1**, 137 (1991).
[20] A. Serfaty de Markus, Phys. Rev. E **55**, 1342 (1997).